Comparison of Ray Tracing and Channel-Sounder Measurements for Vehicular Communications

Jörg Nuckelt*, Taimoor Abbas†, Fredrik Tufvesson†, Christoph Mecklenbräuker‡, Laura Bernadó§ and Thomas Kürner*
*Institut für Nachrichtentechnik, Technische Universität Braunschweig, Braunschweig, Germany
†Dept. of Electrical and Information Technology, Lund University, Lund, Sweden
‡Christian Doppler Lab for Wireless Technologies for Sustainable Mobility, TU Wien, Vienna, Austria
§Forschungszentrum Telekommunikation Wien (FTW), Vienna, Austria

***Abstract*—This paper presents the results of an accuracy assessment of a deterministic channel model for vehicle-to-vehicle (V2V) communications. Channel simulations obtained from the ray-tracing model developed by TU Braunschweig are compared to data gathered during the DRIVEWAY V2V channel measurement campaign at 5.6 GHz in the city of Lund in summer 2009. The analysis focuses on power delay profiles (PDPs) and channel gains in an urban four-way intersection scenario.**

Despite some implementation-based limitations of the ray-tracing model, a very good agreement between simulation and measurement results is achieved. Most relevant power contributions arising from multiple-bounce specular reflections as well as from single-bounce non-specular reflections are captured by the deterministic model. We also discuss the question to what extent roadside obstacles like traffic signs, parked cars or lamp posts have to be considered when characterizing the V2V channel.

I. Introduction

The radio channel poses one of the main challenges of future V2V communication systems. Since the V2V channel differs significantly from well-studied propagation channels of other technologies like cellular networks, many research groups are active in characterizing V2V channel properties. For this reason, there is a need for adequate and reliable channel models allowing a robust and sophisticated system design [1], [2].

In particular, the wave propagation in urban intersection scenarios, where the line-of-sight (LOS) path is typically obstructed by buildings, is strongly limited and affects the reliability of communication in a crucial manner. Some path loss models have been derived from measurements in order to predict the received power in such scenarios [3], [4]. The authors in [4] also introduced parameters like street width and side distance of the transmitting node to surrounding buildings. However, both models assume an intersection with perpendicular side roads and cannot directly be applied to intersections with an irregular geometry.

In order to predict the radio channel of an arbitrary intersection scenario, researchers of TU Braunschweig have developed a ray-optical channel model especially designed for vehicular communications in the 5.9 GHz frequency band [5]. Such a deterministic model easily allows to investigate any desired scenario without carrying out measurements that are costly and require a lot of effort in general. Since the obtained results of ray tracing strongly depend on the implemented mathematical models as well as on the accuracy of the data used to describe the environment, it is necessary to validate the simulations.

Therefore, this paper presents a detailed V2V channel characterization based on ray-tracing simulations and measurement results. The analysis is limited to an intersection scenario, where data from channel sounder measurements carried out in the city of Lund in 2009 is available [6]. We have simulated the scenario under study using the ray-optical channel model of TU Braunschweig and compare the obtained results against measurement data in terms of PDP and path loss metrics. We also deal with the question to what extend obstacles like road signs or parked cars have to be taken into account when characterizing the V2V channel.

This paper is organized as follows: In Section II, we first describe the underlying scenario. Sections III and IV explain the ray-optical channel model and provide information about the V2V measurement campaign, respectively. Simulation results are validated against measurement data in Section V. The results of this paper are finally summarized in Section VI.

II. Urban Intersection Scenario

For the comparison of simulation results against measurement data, we have chosen an urban four-way intersection (N55° 42′ 37″, E13° 11′ 15″, see Fig. 1) in the city of Lund, Sweden. The scenario is exactly the same as the narrow urban scenario described in [7]. The transmitter (Tx) and receiver (Rx) cars are driving through *Karl XII-gatan* and *Spolegatan*, respectively, towards the intersection at a speed of approximately 10 m/s. The LOS component is obstructed by four-

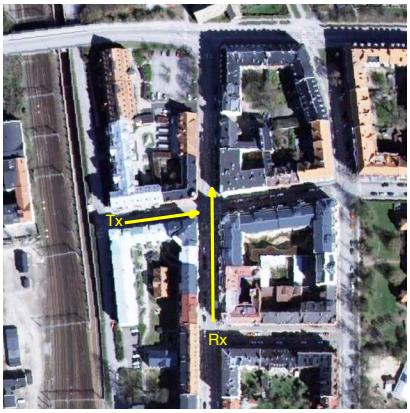

Fig. 1. Aerial image of the investigated urban crossroads scenario in the city of Lund with two vehicles moving towards the intersection at a speed of 30-40 km/h (N55° 42′ 37″, E13° 11′ 15″).

story buildings arranged along each leg of the intersection. The canyon of the street is quite narrow and ranges from 14-17 m. The four side roads are not perfectly perpendicular. During the measurements, vehicles parked along the streets. Furthermore, there were some traffic signs and lamp posts in the close environment of the intersection. It is worth mentioning that a bus was turning left from *Spolegatan* into *Karl XII-gatan* in Western direction at the beginning of the scenario. We will see the impact of this bus later when discussing the results.

III. 3D Ray-optical Channel Model

The underlying simulation-based channel model that is used in this paper belongs to the class of deterministic channel modeling approaches using 3D ray-optical algorithms [5]. In order to characterize the channel between Tx and Rx, the direct path, specular reflections as well as diffuse scattering in terms of non-specular reflections are taken into account. Specular reflections are calculated recursively up to a desired order, but depending on the complexity and level of detail of the environment only reflections up to order three or four are practical regarding the computational effort. Faces of buildings or obstacles that can be seen by both the Tx and the Rx are treated as sources of first-order non-specular reflections, modeled by means of Lambertian emitters. Furthermore, the channel model is able to include the full-polarimetric antenna patterns of Tx and Rx, respectively. It is worth mentioning that the ray-optical channel model does not include diffraction in the horizontal and vertical plane. It is intended to extend the ray tracer by a diffraction model for the horizontal propagation plane. Corner-diffracted radio waves might yield the only power contribution except from non-specular reflections in severe non-line-of-sight (NLOS) situations when Tx and Rx are far away from the intersection center and, therefore, should also be considered in the channel model. However, it is expected that diffraction in the vertical plane caused by propagation over rooftops can be neglected in V2V scenarios.

The output of the ray-optical model is the time-variant channel impulse response (CIR) $h(\tau,t) \in \mathbb{C}^{M_t \times M_r}$, which completely characterizes the frequency-selective channel for each Tx/Rx link for M_t and M_r transmit and receive antennas, respectively. We can express the CIR for single-input single-output (SISO) transmission, i.e. $M_t = M_r = 1$, as

$$h\left(\tau,t\right) = \sum_{k=1}^{N(t)} a_k\left(t\right) \cdot e^{j(2\pi f \tau_k(t) + \varphi_k(t))} \cdot \delta(\tau - \tau_k(t)) \quad (1)$$

$$= \sum_{k=1}^{N(t)} \underline{a}_k\left(t\right) \cdot \delta(\tau - \tau_k(t)), \quad (2)$$

where the k-th multipath component is described by an amplitude $a_k(t)$, a delay $\tau_k(t)$ and an additional phase shift $\varphi_k(t)$ at time t. $N(t)$ denotes the time-variant number of multipath components. Based on the predicted CIRs further metrics like the PDP, the channel gain or the root mean square (RMS) delay spread can be derived and compared with measurement-based data.

In order to characterize the wireless V2V channel using the ray-tracing techniques, the investigated scenario has to be described in terms of all buildings and obstacles that mainly interact with the transmitted signal and, therefore, affect the wave propagation. We obtain building data from the OpenStreetMap database[1]. Since the height of the buildings around the considered intersection is not available in the database, we define a fixed height of 15 m for all buildings. The specific height seems not critical in this peer-to-peer scenario as most propagation processes take place at street level. By analyzing the videos captured during the measurements and on-site inspections of the intersection, we identify relevant obstacles like traffic signs, lamp posts or parked cars along the roadside and add these objects in a simplified way with less details to the virtual scenario. The trajectories of the moving Tx and Rx, respectively, are reproduced using the GPS coordinates logged during the measurement runs. Finally, the snapshot-based CIRs at a time resolution of 10 ms are calculated by the channel model. A post-processing algorithm that exploits knowledge about the positions of Tx, Rx and scatterers as well as the driving speed of the vehicles interpolates afterwards the obtained CIR data between two adjacent snapshots leading to a final time resolution of $100\,\mu$s. As an example, Fig. 2 illustrates the virtual scenario and visualizes the calculated propagation paths of an arbitrary snapshot.

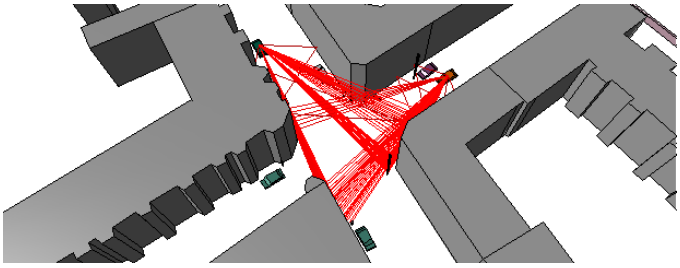

Fig. 2. Simulation of the underlying urban intersection scenario by means of ray tracing. The data of the environment includes buildings, traffic signs, lamp posts as well as parked cars along the roadside.

IV. Channel Measurement Setup

The RUSK Lund channel sounder, which performs the multiple-input multiple-output (MIMO) measurements based on switched array principle, was used to record the complex time-varying channel transfer function $H(f,t)$. The corresponding CIR $h\left(\tau,t\right)$ is derived from $H(f,t)$ by applying an inverse Fourier transform. For each measurement, the sounder sampled the channel for 10 s using time increment of $\Delta t = 307.2\,\mu$s at a carrier frequency of 5.6 GHz and a bandwidth of 240 MHz. Two regular hatchback cars, with a height of 1.73 m, each equipped with a four-element antenna array were used to perform V2V measurements. These antenna arrays, integrated into existing radomes ('shark fin') on the car roof, were specifically designed for V2V communications with omni-directional array pattern in azimuth. The interested reader is referred to [6], where a detailed description of the measurement set up can be found.

V. Comparison of Simulations and Measurements

A. Power Delay Profile

We calculate the time-variant PDP of the channel based on measurement data and simulation results, respectively, as

$$P_\tau(\tau,t) = \frac{1}{N_t} \sum_{n=0}^{N_t-1} |h(\tau, t+n\Delta t)|^2, \quad (3)$$

[1]See www.openstreetmap.org for more information.

where the CIRs are averaged over a window of $N_t \Delta t = 57\,\mathrm{ms}$ corresponding to a distance of 10 wavelengths at a Tx or an Rx speed of 35 km/h. Note that there is an additional averaging of all 4x4 MIMO links of the measured channel data in order to minimize the directional impact of the antenna pattern. Furthermore, the processing includes a noise reduction of the measurement data described in [7]. The resulting PDP of the measurement and the simulation are depicted in Fig. 3 and 4. At first sight, we find a good agreement when comparing the simulated PDP against the measurement data. Several multipath components (MPCs) can be identified in both figures. However, there are individual discrete as well as diffuse scatterers that can be found in the measured PDP but not in the simulated one and vice versa. In the following, the observed differences will be discussed in more detail.

In the very first seconds of the scenario in the absence of LOS between Tx and Rx, a bus was turning left, from *Spolegatan* into *Karl XII-gatan*. Due to the alignment of Tx, bus and Rx, a very good scatterer arises in the center of the intersection leading to the contribution (a) in Fig. 3. Since the bus as a moving object was not included in the simulation we cannot observe this MPC in Fig. 4. In the time interval from 2 to approximately 5 s, the bus was driving into the direction of the Tx. Hence, the LOS to a building near the intersection center that would have caused first-order non-specular reflections was obstructed by the bus. This explains why power contribution (b) cannot be observed in Fig. 3 but in Fig. 4 since the LOS to the building is not obstructed by the bus in the simulation.

Approximately at time 6.5 s the Tx and Rx are very close to the intersection, and the LOS component (c) appears in both figures for the first time. Furthermore, the group of arrows (d) point at several strong MPCs induced by specular and non-specular reflections of the first order that probably come from the surrounding buildings. There are some power contributions (e) and (f) that can be observed in the measurement, but not in the simulation. The path lengths of contributions (f) range from 170 up to 250 m, whereas the distance is constant with respect to time. By contrast, the component corresponding to (e) seems to be a moving object, as the distance increases with time. We calculate the scattering ellipses for these four discrete MPCs in the time interval from 7.5 to 9 s that are depicted in Fig. 5.

Based on these results and observation of the videos of the measurement, MPC (e) is doubtless originated by the moving bus that has passed the Tx in the *Karl XII-gatan* and is still visible in the time interval from 7.5 to 9 s. More surprisingly, we have identified a wall, a pylon of a power line as well as a high building on the other side of the railway that lead to the contributions of (f). Since neither the bus nor the other objects were included in the simulated scenario, their impact cannot be observed in the PDP.

The static objects corresponding to power contributions (f) have been added to the scenario. Due to limitations of simulations, the moving bus is not included. The obtained PDP of the extended scenario is shown in Fig. 6. It can be observed that the ray tracer captures the impact of the added MPCs and now the missing power contributions appear also in the simulated PDP. The underestimation of the long delayed

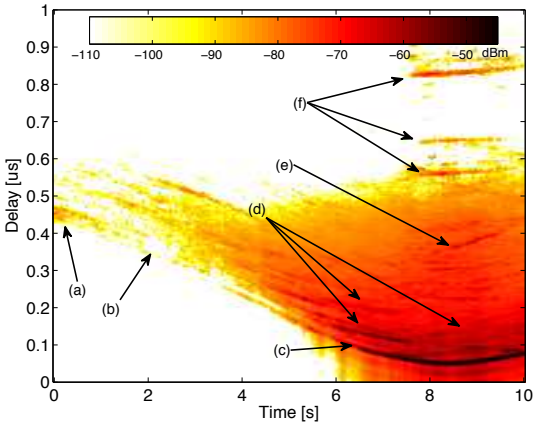

Fig. 3. Power delay profile based on channel sounder data averaged over all 4x4 MIMO links.

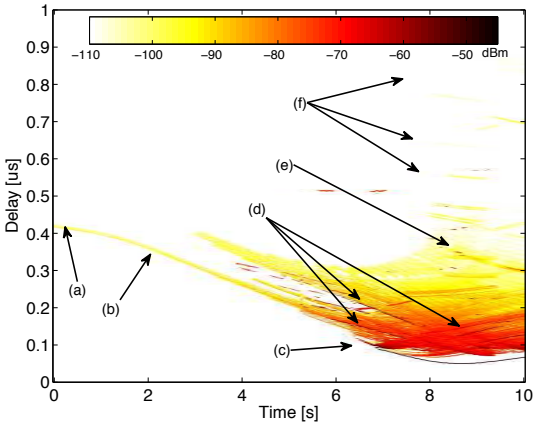

Fig. 4. Power delay profile obtained from the predicted CIRs using the ray-tracing channel model.

contribution caused by the high building can be explained by the material of its walls. After an on-site inspection of the intersection including this building we have found that walls of this building are made by corrugated iron. The combination of many nooks and a metallic surface causes a very good source of specular and non-specular reflections of first and higher orders. However, such specific effects that are caused by some detailed characteristics of the environment cannot be captured by the ray tracer.

In addition to the aforementioned discrete MPCs, we can observe a lot of diffuse scattering with larger delays in the measured PDP. These diffuse scatterers do not appear in the simulation results since the ray tracer does not take non-specular reflections of higher orders into account, i.e. the combination of a specular reflection and non-specular reflection, for example, is not implemented in the channel model. It is also worth mentioning that some general blurring effects due to the post-processing of the measurement data become visible in the corresponding PDP figure.

B. Channel Gain

Based on the PDP, we calculate the time-variant channel gain including the impact of the used antennas and the system loss as

$$G(t) = \sum_{\tau} P_{\tau}(\tau, t). \tag{4}$$

Fig. 7 presents the predicted channel gains obtained from ray-tracing simulations and measurement data. Simulations have been carried out up to reflection order four. The depicted channel gains correspond to a plain scenario, where all roadside obstacles like traffic signs, lamp posts and also the parked cars have been removed in order to reduce the simulation time. Note that we have compared the simulation results of the complex scenario including roadside obstacles with the plain scenario and found only marginal differences in the channel gain values (see also Table I).

In Fig. 7, we can observe a very good agreement of simulation and measurement results in the LOS region ($t \geq 6.8\,\mathrm{s}$) and in the transition from NLOS to LOS ($5.7\,\mathrm{s} \leq t < 6.8\,\mathrm{s}$). The most relevant power contributions arise from the LOS component and first-order specular and non-specular reflections that are captured by the ray tracer. We can observe a gap between measurement and simulation in the severe NLOS period ($t < 5.7\,\mathrm{s}$) of approximately 8 to 10 dB, whereas the ray-optical channel model underestimates the channel gain. As expected, the agreement between measurement and simulation depends strongly on the order of specular reflections that is taken into account. We can improve the accuracy of the channel gain predictions by increasing the reflection order that is handled by the ray tracer at the cost of a higher computational time.

Fig. 8 shows the relative contribution of the LOS path and higher-order specular reflections and non-specular reflections of the first order. The strongest power contribution (60-85 %) arises from the LOS path if it is present. The remaining received power is mainly originated from first-order specular and non-specular reflections due to buildings since obstacles like traffic signs, etc. are not included in this simulation. We have also analyzed the power contribution in this scenario including the roadside obstacles and have observed a partly increased power contribution (approx. 5 %) of specular and non-specular reflections. These results are in a very good agreement of the work presented in [8]. Applying the SAGE algorithm in order to identify the most relevant MPCs, the authors in [8] have calculated a relative power contribution of

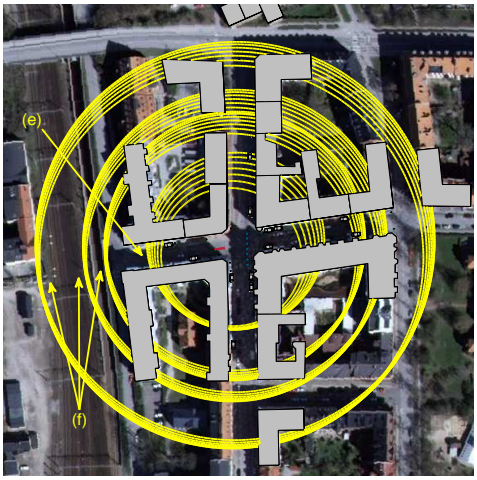

Fig. 5. Scattering ellipses of the MPC denoted by (e) and (f) in Fig. 3. Positions of the Tx and Rx are marked by the red and blue dots, respectively. The corresponding time is from 7.5 to 9 s.

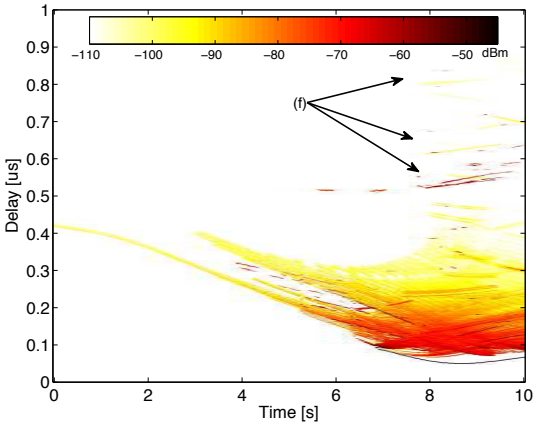

Fig. 6. Simulated power delay profile of the intersection scenario extended by missing MPCs (a wall, a pylon and a building) located in the western region of the scenario.

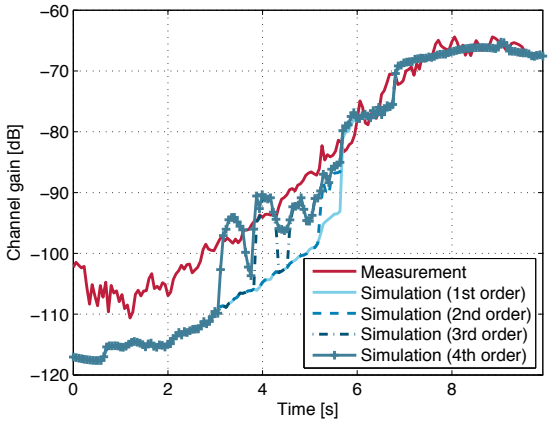

Fig. 7. Measured versus simulated channel gains of the plain scenario for different reflection orders that have been taken into account.

the LOS component between 70 and 80 %.

Regarding the NLOS period of the scenario, we observe only higher-order reflections, whereas first- and second-order specular reflections do not have any significant impact. This is reasonable due to the geometrical arrangement of Tx, Rx and the surrounding buildings. This part of the figure also demonstrates the limitations of the ray-optical channel model. Up to time 3 s, the current channel model can only calculate non-specular reflections that arise from scattering interactions of the first order. Higher-order non-specular reflections are currently not included in the channel model which leads to the

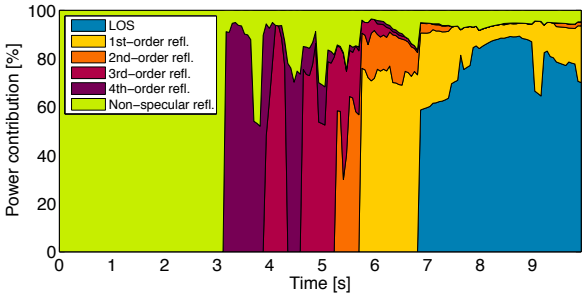

Fig. 8. Relative power contribution in the simulated plain scenario of LOS, up to 4th-order specular reflections and 1st-order non-specular reflections.

TABLE I
MEAN ERROR μ AND STANDARD DEVIATION σ OF THE SIMULATED AND MEASURED CHANNEL GAIN OF THE PLAIN SCENARIO. VALUES IN BRACKETS CORRESPOND TO THE COMPLEX SCENARIO INCLUDING OBSTACLES AS PARKED CARS AND TRAFFIC SIGNS.

Reflection order	LOS		NLOS	
	$\mu\,[dB]$	$\sigma\,[dB]$	$\mu\,[dB]$	$\sigma\,[dB]$
1st	0.17 (-0.12)	1.24 (1.49)	8.88 (8.15)	4.28 (4.19)
2nd	0.12 (-0.24)	1.30 (1.51)	8.44 (7.67)	4.45 (4.27)
3rd	0.11 (-0.26)	1.30 (1.52)	6.80 (6.12)	5.01 (4.71)
4th	0.11 (N/A)	1.30 (N/A)	5.38 (N/A)	5.34 (N/A)

mismatch between measurement and simulation. At snapshots where the ray tracer identifies higher-order specular reflections, this gap is clearly reduced (cf. Fig. 7 and 8). However, some further improvements of the model are needed to take also higher-order non-specular reflections into account.

Finally, Table I shows the mean error

$$\mu = \mathrm{E}\left[G_{\mathrm{meas}} - G_{\mathrm{sim}}\right] \tag{5}$$

and the standard deviation

$$\sigma = \sqrt{\mathrm{E}\left[\left|\mu - G_{\mathrm{sim}}\right|^2\right]} \tag{6}$$

between simulated and measured channel gains. The values distinguish between LOS and NLOS and are given for different reflection orders. The values correspond to the plain scenario, where roadside obstacles are not included (cf. Fig. 7). The values belonging to the complex scenario including roadside obstacles are given in brackets.[2] We find a strong agreement in the LOS part. Both, mean error and standard deviation of the model are less than or around 1 dB which are very good results. Regarding the NLOS part we obtain a higher mean error up to approximately 9 dB. When increasing the order of specular reflections that are taken into account, the mean error can be reduced up to 5.4 dB. It is obvious that the ray tracer underestimates the channel gain as higher-order non-specular reflections are not considered. Hence, the mean error in NLOS regions can be further reduced by extending the channel model to higher-order non-specular reflections. Note that the measured channel gain includes also the positive effects of the left-turning bus at the beginning of the scenario. Since this moving object is not included in the simulation, there is another mismatch, of several dB, between simulations and measurements for this specific scenario. We have also found that the inclusion of roadside obstacles does not have any major impact on the total gain. Mean error and standard deviation of the plain and the complex scenario do not differ significantly. Roadside obstacles, however, have shown to be very noticeable scatterers in more sparse environments like highways.

VI. CONCLUSION

In this paper, we have presented an analysis of V2V channels in an urban intersection scenario. We have compared metrics like channel gain and PDP that are obtained from channel sounder measurements and raytracing simulation. We have found a very good accuracy of the channel model as far as the present physical phenomena of wave propagation are captured by the implemented algorithms. Variations between measurements and simulations are consistent and can be explained with the microscopic features of the investigated scenario. We have identified limitations of the channel model in terms of higher-order non-specular reflections that are currently not included. The conducted evaluation has revealed that power contributions arising from non-specular reflections of higher orders cannot always be neglected. Especially under NLOS conditions, these multi-bounce non-specular reflections might provide the solely power contribution at the Rx. We have also found that roadside obstacles like traffic signs or parked cars do not have a significant impact on the total received power. Nevertheless, they probably cannot be ignored when considering MIMO and spatial diversity. For this reason, future work will take these new insights into account to enhance the ray-optical channel model and increase its accuracy in severe NLOS channels.

[2]Due to the high computational effort of the complex scenario, results for fourth-order reflections could not be obtained in a reasonable amount of time

ACKNOWLEDGMENT

This work has been carried out in close collaboration between TU Braunschweig and Lund University within the COST IC 1004 framework. The authors would like to thank the IC 1004 committee for supporting and funding this short-term scientific mission. We would also like to thank Delphi Delco Electronics Europe GmbH for designing the antennas used for the DRIVEWAY measurements. Laura Bernadó is funded by the Vienna Science and Technology Fund in the FTW project NOWIRE. The Competence Center FTW is funded within the program COMET by BMVIT, BMWFJ, and the City of Vienna. The COMET program is managed by the FFG. Christoph Mecklenbräuker is partially funded by Christian Doppler Forschungsgesellschaft.

REFERENCES

[1] A. Molisch, F. Tufvesson, J. Karedal, and C. Mecklenbräuker, "A survey on vehicle-to-vehicle propagation channels," *IEEE Wireless Communications*, vol. 16, no. 6, pp. 12–22, December 2009.

[2] R. Santos, A. Edwards, and V. Rangel-Licea, *Wireless Technologies in Vehicular Ad Hoc Networks: Present and Future Challenges*. IGI Global, 2012.

[3] M. Schack, J. Nuckelt, R. Geise, L. Thiele, and T. Kürner, "Comparison of path loss measurements and predictions at urban crossroads for C2C communications," in *5th European Conference on Antennas and Propagation (EuCAP)*, April 2011.

[4] T. Mangel, O. Klemp, and H. Hartenstein, "A validated 5.9 GHz Non-Line-of-Sight path-loss and fading model for inter-vehicle communication," in *11th International Conference on ITS Telecommunications (ITST)*, August 2011.

[5] J. Nuckelt, M. Schack, and T. Kürner, "Deterministic and stochastic channel models implemented in a physical layer simulator for Car-to-X communications," *Advances in Radio Science*, vol. 9, pp. 165–171, September 2011.

[6] A. Paier, L. Bernadó, J. Karedal, O. Klemp, and A. Kwoczek, "Overview of Vehicle-to-Vehicle Radio Channel Measurements for Collision Avoidance Applications," in *71st IEEE Vehicular Technology Conference (VTC)*, May 2010.

[7] J. Karedal, F. Tufvesson, T. Abbas, O. Klemp, A. Paier, L. Bernadó, and A. Molisch, "Radio channel measurements at street intersections for vehicle-to-vehicle safety applications," in *71st IEEE Vehicular Technology Conference (VTC)*, May 2010.

[8] T. Abbas, J. Karedal, F. Tufvesson, A. Paier, L. Bernado, and A. Molisch, "Directional analysis of vehicle-to-vehicle propagation channels," in *73rd IEEE Vehicular Technology Conference (VTC)*, May 2011.